

pubs.acs.org/macroletters Letter

Unraveling Depth-Specific Ionic Conduction and Stiffness Behavior across Ionomer Thin Films and Bulk Membranes

Seefat Farzin, Ehsan Zamani, and Shudipto K. Dishari*



Cite This: ACS Macro Lett. 2021, 10, 791–798



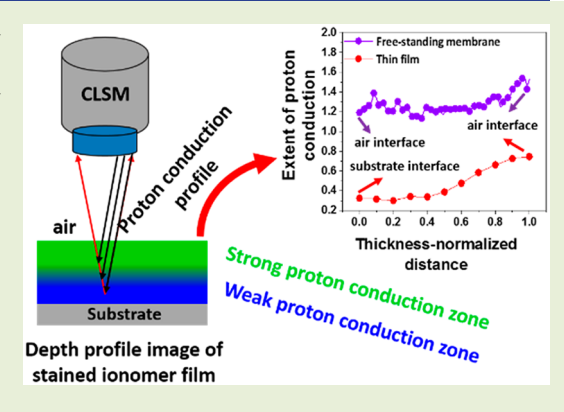
ACCESS

Metrics & More

Article Recommendations

Supporting Information

ABSTRACT: Interfacial behavior of submicron thick polymer films critically controls the performance of electrochemical devices. We developed a robust, everyday-accessible, fluorescence confocal laser scanning microscopy (CLSM)-based strategy that can probe the distribution of mobility, ion conduction, and other properties across ionomer samples. When fluorescent photoacid probe 8-hydroxypyrene-1,3,6-trisulfonic acid trisodium salt (HPTS) was incorporated into <1 μ m thick Nafion films on substrates, the depth-profile images showed thickness- and interface-dependent proton conduction behavior. In these films, proton conduction was weak over a region next to substrate interface, then gradually increased until air interface at 88% RH. Conversely, consistently high proton conduction with no interface dependence was observed across 35–50 μ m thick bulk, free-standing Nafion membranes. A hump-like mobility/stiffness distribution was observed across Nafion films containing mobility-sensitive probe (9-(2-carboxy-2-cyanovinyl)-



julolidine) (CCVJ). The proton conduction and mobility distribution were rationalized as a combinatorial effect of interfacial interaction, ionomer chain orientation, chain density, and ionic domain characteristics.

As the demand for thinner electrochemical devices increases, ionomer confinement, and interfacial phenomena studies become more critical. These studies are of high relevance to proton exchange membrane fuel cells in which the ion conduction limitation within a submicron thick ionomer (like Nafion, Figure 1a) layer at catalyst interface slows down the electrochemical reaction. While the properties of bulk, free-standing, several tens of μ m-thick ionomer membranes have been explored extensively, the understanding of ionomer thin films (<1 μ m thick) is still inadequate. The continued efforts to unravel thin film behavior have made it evident that the proton conductivity of submicron thick ionomer films are influenced in a complex manner by parameters such as hydrophilic—hydrophobic phase separation; 12,111 spacing, and connectivity; 12,111 spacing, and connectivity; 14,112 water—ionomer mobility 15,6,11,13 and orientation; 2,14,115 water—ionomer—substrate interfacial interactions; 16,16

Fluorescent dyes have made an unprecedented improvement of our understanding of confined/nanoscopic systems by revealing (i) glass transition temperature, $T_{\rm g}$ (pyrene-based dyes); $^{19-21}$ (ii) water diffusion coefficient, 22 viscosity, $^{23-25}$ mobility, 11,24,25 and stiffness 5,6,11,13,26,27 (rotor probes); (iii) proton transport dynamics, $^{28-32}$ proton concentration, 6,12,33 and ionic domain size 12 (photoacid probes); and many other properties. Earlier, we incorporated a fluorescent photoacid probe HPTS (Figure 1b, top) within ionomer samples. 6,8,12 HPTS is sensitive to the local proton conduction environment and exhibits ratiometric fluorescence response ($I_{\rm d}/I_{\rm p}$). At the

electronically excited state, the pK_a of HPTS decreases from 7.7 to 0.7. The excited dye can donate its phenolic proton, stay deprotonated (I_d) and show an increased value of deprotonation ratio (I_d/I_P) only if the neighboring water molecules are favorable for carrying the protons away from the protongeneration sites. Using steady-state fluorescence spectroscopy, we therefore obtained an average value of $I_{\rm d}/I_{\rm p}$ for an entire sample as an indirect measure of the extent of proton conduction. 6,8,12,32,33 Additionally, HPTS helps to extract information about critical parameters of the local hydration environment (ionic domain size, acidity)^{6,8,12,33} that give rise to the quantitative value of proton conductivity (σ) of a sample, measured using electrochemical impedance spectroscopy (EIS).3 HPTS also allowed us to estimate the average ionic domain size which closely matched with what was obtained using grazing-incidence small-angle X-ray scattering¹² and demonstrated the reliability of fluorescence-based techniques.

Earlier, we employed CCVJ (Figure 1b, bottom) within ionomer thin films that can respond to dimensional constraint-

Received: February 23, 2021 Accepted: June 8, 2021 Published: June 10, 2021





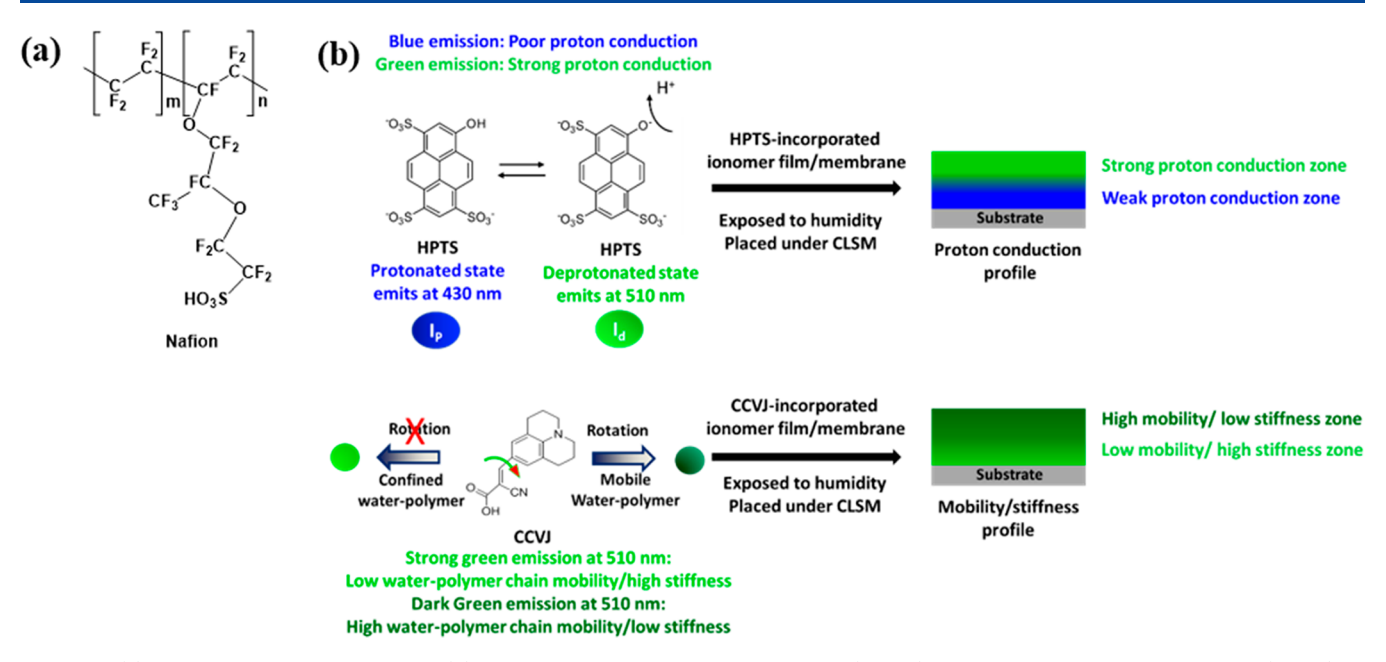


Figure 1. (a) Chemical structure of Nafion; (b) working principles of photoacid probe (HPTS) and mobility-sensitive rotor probe (CCVJ) to obtain depth-specific ion conduction in thin films and membranes using CLSM. Here, $I_{\rm d}$ and $I_{\rm p}$ are the emission intensities of HPTS at deprotonated ($\lambda_{\rm em,max} \sim 510$ nm) and protonated ($\lambda_{\rm em,max} \sim 430-440$ nm) states, respectively.

induced restriction in water-polymer mobility, waterpolymer-substrate interaction-induced film stiffening, or both. 6,13,5,11 In a stiff/confined environment where rotation around the bond between electron donor and acceptor parts of CCVJ is restricted, CCVJ emits strong green fluorescence. But if CCVI resides in a less stiff/more mobile environment, this bond rotation within CCVJ leads to charge transfer and fluorescence quenching of CCVJ. By incorporating CCVJ, we revealed the following about ionomeric systems: (i) films <1 μ m lost water-polymer mobility and stiffened upon hydration; ^{5,6} (ii) water-ionomer mobility, when sacrificed, proton conductivity became poor; 11 (iii) antiplasticization dynamics (time-resolved fluorescence) suggested a possible presence of distributed mobility within ionomer films which rationalized the water—polymer mass distribution across the films. ^{13,34,35} Fluorescence ^{19,20,36} and ellipsometric ³⁷ measurements are often done to explore the distribution of T_g in thin films. Such distributions can lead to distribution in the proton conduction environment across ionomer films. Techniques, like, neutron reflectometry, ^{13,34,35,38,39} X-ray computed tomography, 40,41 cryo-TEM tomography, 10 and resonant soft X-ray scattering 42-44 have elucidated the mass/density distribution, 13,34,35,38-41 three-dimensional chemical 42 and nanostructure turn, within heterogeneous materials. But these instruments are not frequently accessible for everyday experimentation. Importantly, ion conduction³ and mechanical properties, 18 the two most critical performance parameters of ionomers, are still reported as an average value for an entire sample. We thus need strategies to reveal the distribution of these two properties across ionomer samples.

Here, we report a robust, versatile strategy using CLSM to unravel the depth-specific properties of ionomers in both bulk membrane and thin-film format. CLSM is an everyday-accessible instrument that can capture two-dimensional (xy-plane) fluorescence images at different depths within a sample containing fluorescent molecules. A depth profile image is obtained by z-stacking these xy-plane images. This depth-

profile image thus represents the fluorescence response along with the thickness of the material. When we took CLSM images of Nafion films and bulk membranes containing HPTS under controlled relative humidity (% RH), the $I_{\rm d}/I_{\rm p}$ profile revealed the distribution of proton conduction across hydrated ionomer samples (Figure 1b, top). We also did a similar CLSM measurement, but with CCVJ to obtain the distribution of mobility/stiffness (Figure 1b, bottom) across the same ionomer samples.

We measured both σ (EIS, Figure S1) and $I_{\rm d}/I_{\rm p}$ (steady-state fluorescence spectroscopy, Figure S2) of Nafion films. For bulk membrane, we measured $I_{\rm d}/I_{\rm p}$, while took the σ value from literature ⁴⁵ at similar conditions. The curve shows a decent correlation between $I_{\rm d}/I_{\rm p}$ and σ (Figure 2). This correlation proved that the fluorescence-based techniques, despite being qualitative, provide reliable information which can help to

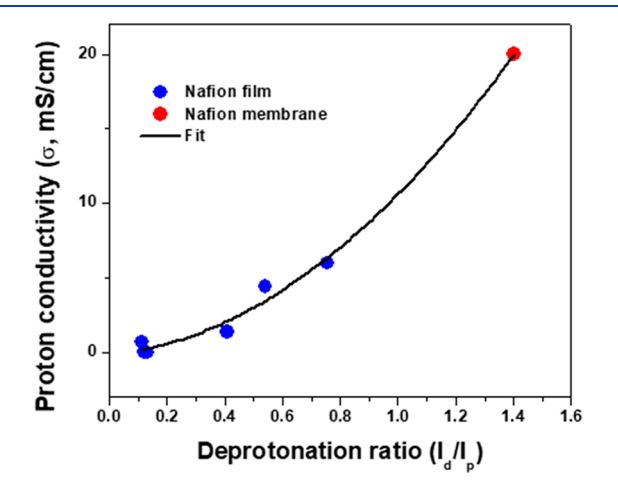


Figure 2. Correlation between deprotonation ratio $(I_{\rm d}/I_{\rm p})$, measured using fluorescent photoacid probe HPTS and steady-state fluorescence spectroscopy) and quantitative value of proton conductivity $(\sigma,$ measured using EIS).

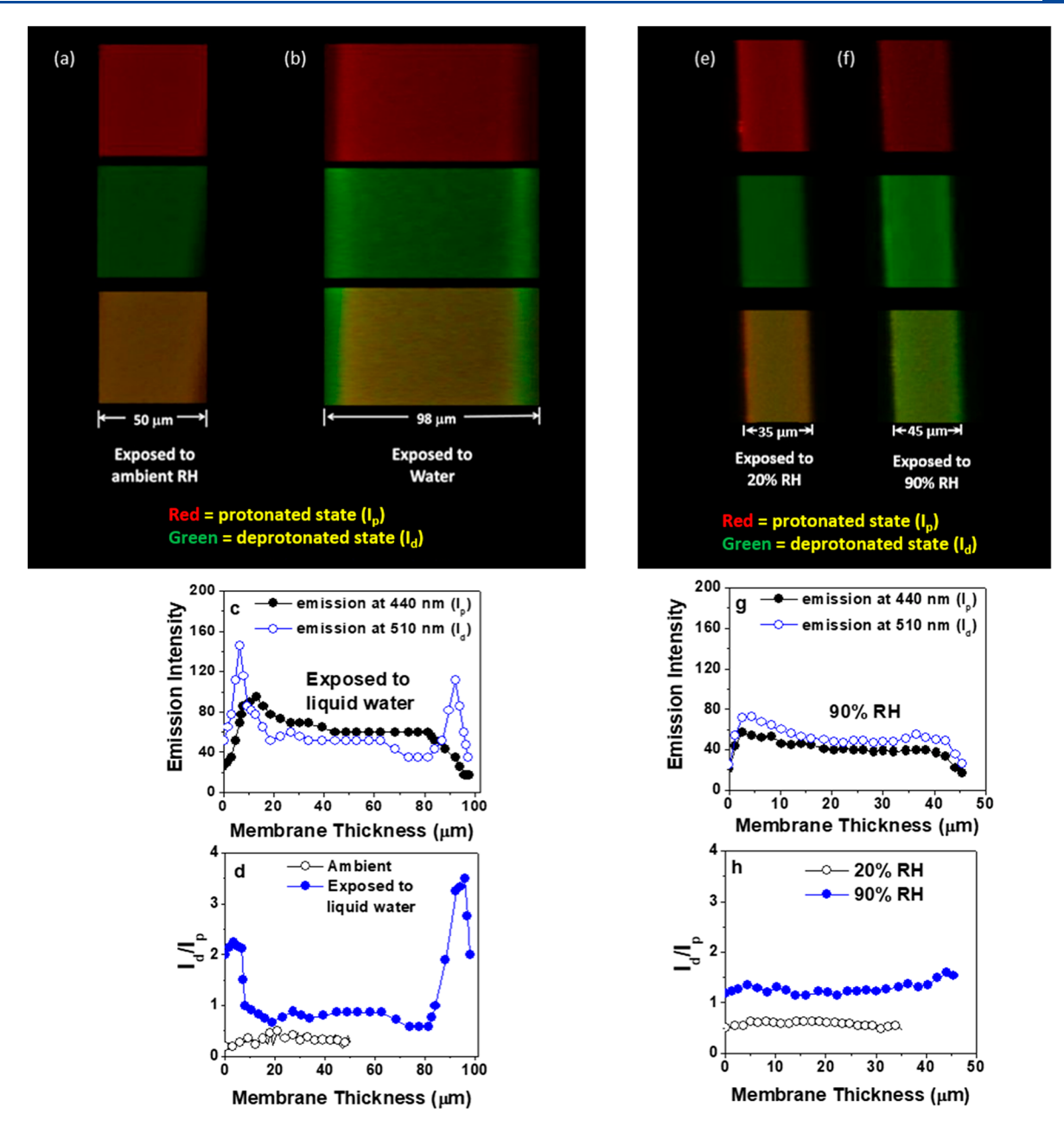


Figure 3. CLSM images (pseudocolored) of an annealed Nafion (NR 212) membrane with HPTS taken in ambient air (\sim 20% RH, measured using RH probe) (a), and after a quick dipping in liquid water (b). CLSM images of another annealed Nafion membrane exposed to 20% RH (e) and 90% RH (f). The membrane was equilibrated at each RH for 2 h. Since the blue (I_p) and green (I_d) emissions of HPTS are difficult to differentiate visually, we used red (a, b, e, f - top row) and green (a, b, e, f - mid-row) as pseudocolors to represent the emission of protonated (I_p) and deprotonated (I_d) states of HPTS, respectively. The bottom rows of these images (a, b, e, f) were obtained by superpositioning both red and green color channels for a sample. I_d and I_p profiles are shown for water-dipped (c) and humidified (g) membranes. Corresponding I_d/I_p profiles are also shown (d, h) in comparison with those at ambient or low humidity (20% RH) conditions. The CLSM images showed that the thickness of the Nafion membranes used for these two sets of measurements was different at ambient conditions. The membrane thicknesses were reconfirmed using Vernier calipers and the differences in thickness were attributed to the roll-to-roll variation of purchased membranes. The thickness increase of wet (b) and humidified (f) membranes represents hydration-induced swelling. All these experiments were repeated three times.

understand the quantitative values of σ . Also, this correlation curve and CLSM-based $I_{\rm d}/I_{\rm p}$ profile together allowed us to predict the σ value at different depths within ionomer films/membranes.

Our first, proof-of-concept CLSM experiment was with an HPTS-incorporated Nafion membrane. After imaging the membrane at ambient condition (\sim 20% RH; Figure 3a), it was dipped into liquid water for 5 s and reimaged (Figure 3b–d). At ambient conditions, we obtained bright red (I_n ; Figure

3a, top) and faint green ($I_{\rm d}$; Figure 3a, mid) z-stacked images. The corresponding $I_{\rm d}/I_{\rm p}$ profile showed a consistently low value ($I_{\rm d}/I_{\rm p}\sim0.35$) across the membrane. This indicated a uniform, but weak proton conduction environment across the membrane at 20% RH. After quick-dipping in water, about $10-15~\mu{\rm m}$ region on each side of the membrane showed faint red (Figure 3b, top) and bright green (Figure 3b, mid) emission. In the superpositioned image (Figure 3b, bottom), these two edges of the membrane were yellowish-green, while

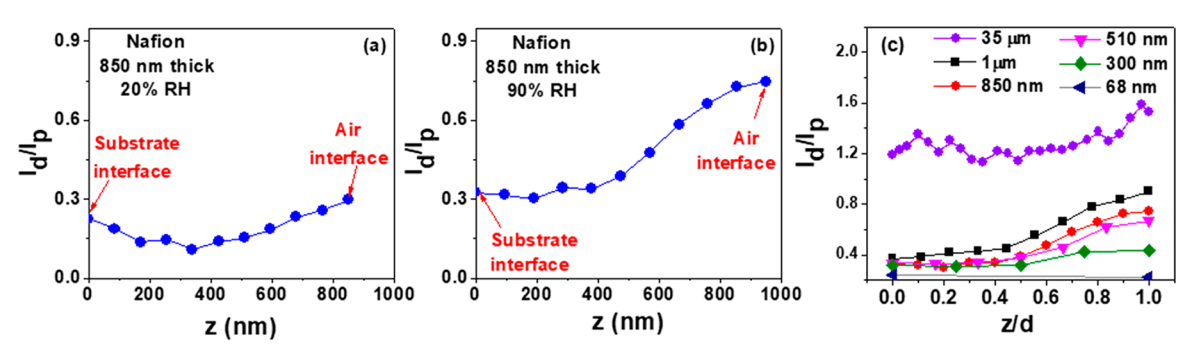


Figure 4. $I_{\rm d}/I_{\rm p}$ profile of HPTS across an 850 nm thick, annealed Nafion film at 20% (a) and 90% RH (b). Here, z is the distance within the film from the substrate interface. (c) $I_{\rm d}/I_{\rm p}$ profiles as a function of film thickness (d)—normalized distance (z) from substrate interface (z/d) for 68—1000 nm thick Nafion films on glass coverslips (having SiO₂ on the surface) and 35 μ m thick free-standing Nafion membrane at 90% RH. All these experiments were repeated three times.

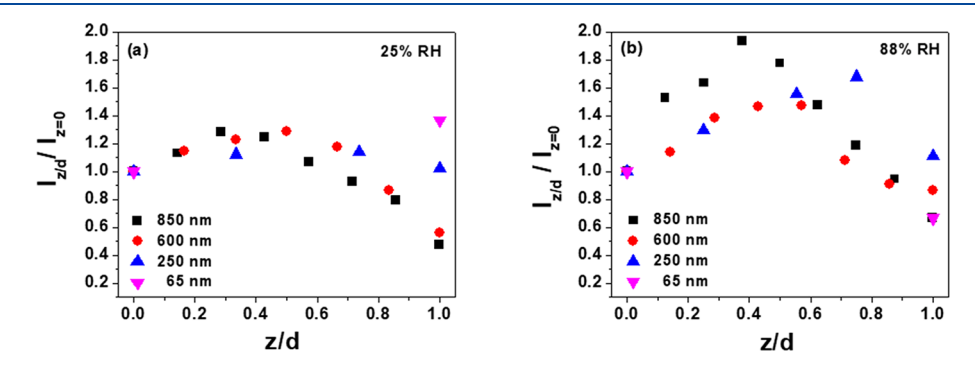


Figure 5. Fluorescence response of CCVJ ($\lambda_{\text{exc,max}}$ = 440 nm, $\lambda_{\text{em,max}}$ = 510 nm) across 65–850 nm thick, annealed Nafion films at (a) 25% RH and (b) 88% RH. Here, $I_{z/d}$ indicates the emission intensity at a certain z/d value; and $I_{z/d}/I_{z=0}$ represents the fluorescence intensity of CCVJ at a certain depth ($I_{z/d}$) within a Nafion film as compared to that right next to substrate interface ($I_{z=0}$) at the same %RH. All these experiments were repeated three times.

the mid-region (\sim 70 μ m) was orangish-red. Because of quickly dipping in water, water diffusion deep down into the membrane did not occur, and only a small region next to the air interface of the membrane was wetted. This rationalized the sharp increase in $I_{\rm d}/I_{\rm p}$ (\sim 2.25–3.5) at the two edges and the relatively flat, low-lying $I_{\rm d}/I_{\rm p}$ (\sim 0.84) profile in the middle of this membrane (Figure 3d). This experiment demonstrated the feasibility of the CLSM-based approach to obtain polymer properties across the sample.

We then exposed an HPTS-incorporated Nafion membrane to humid air in a humidity-controlled chamber (Figure S3) and imaged it at 20% (Figure 3e) and 90% RH (Figure 3f–h). The superpositioned image showed orange emission (Figure 3e, bottom) and indicated weak $I_{\rm d}/I_{\rm p}$ across the membrane at 20% RH. At 90% RH, this orange image turned yellowish-green color with a dominance of green uniformly throughout the membrane (Figure 3f, bottom). $I_{\rm d}/I_{\rm p}$ value was relatively low (~1.3, Figure 3h) when humid air was used instead of liquid water and agreed with different membrane hydration and ionomer self-assembly 47,48 achieved by these two hydration methods. Additionally, the σ value corresponding to $I_{\rm d}/I_{\rm p}\sim 1.3$ was ~17.44 mS/cm (Figure 2), which was close to that of bulk membrane at similar conditions.

We then CLSM-imaged 65–1000 nm thick films (containing HPTS) on the substrates at 20% and 90% RH (Figure 4). The concentration of HPTS in ionomer suspension and the z-interval for xy-scanning were chosen based on systematic studies of their effects on $I_{\rm d}/I_{\rm p}$ profile (Figures S4 and S5). The CLSM images of representative Nafion thin films are shown in Figure S6.

An 850 nm thick Nafion film at 20% RH showed a relatively flat profile with $I_{\rm d}/I_{\rm p}\sim 0.12-0.22$ (Figure 4a) and indicated consistently low $I_{\rm d}/I_{\rm p}$ across the film at low humidity. At 90% RH, the $I_{\rm d}/I_{\rm p}$ profile stayed flat at a value ~ 0.33 up to ~ 400 nm distance (z) starting from substrate interface, then gradually increased up to $I_{\rm d}/I_{\rm p}\sim 0.76$ at the air interface (Figure 4b). The corresponding σ values from the correlation curve (Figure 2) supported weaker proton conductivity across submicron thick films (~ 1.60 and ~ 8.87 mS/cm at the substrate and air interfaces of 850 nm thick film, respectively) as compared to the bulk membrane (~ 17.44 mS/cm).

When we plotted $I_{\rm d}/I_{\rm p}$ as a function of distance fraction z/d (Figure 4c), we saw that in all the films, a low $I_{\rm d}/I_{\rm p}$ region propagated up to about half the depth of the films from the substrate interface $(z/d\sim 0.5)$. $I_{\rm d}/I_{\rm p}$ then gradually increased and showed the highest value right next to the air interface (z/d=1). The $I_{\rm d}/I_{\rm p}$ at the air interface was thickness-dependent and increased as films became thicker. While submicron thick, supported Nafion films showed interface-dependent proton conduction behavior, bulk Nafion membrane, having no confining substrate interface, had a more favorable and almost uniform ion conduction environment $(I_{\rm d}/I_{\rm p}\sim 1.2-1.4)$ across the membrane (Figure 4c). The $I_{\rm d}/I_{\rm p}$ profiles thus clearly showed the role of thickness and interface on ionic conduction.

Neutron reflectometry measurements suggested water accumulation near the substrate interface of submicron thick ionomer^{13,38,39} films; while our CLSM images suggested that the water molecules residing near the substrate interface are likely not conducting protons efficiently. This can happen if the water molecules and ionomer chains near the substrate

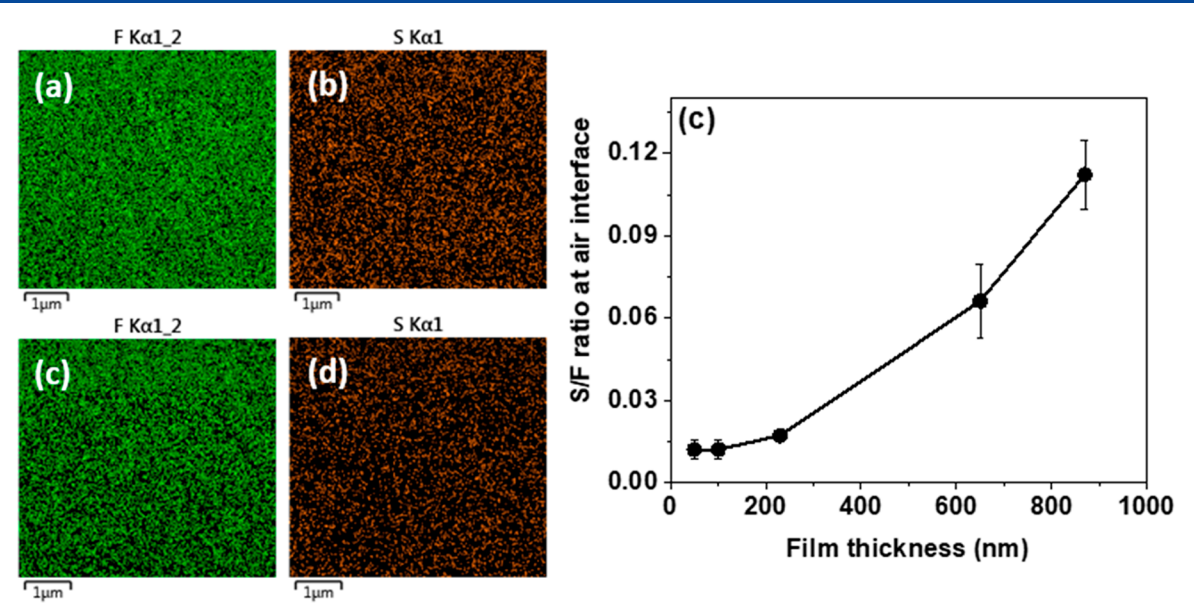


Figure 6. Fluorine (a, c) and sulfur (b, d) elemental map at the air interface of 850 nm thick (a, b) and 230 nm thick (c, d) annealed Nafion films. Sulfur-to-fluorine (S/F) ratio (with standard deviation) at the air interface as a function of Nafion films (e). The chemical mapping experiment was performed three times for each film.

interface are not mobile enough to favor local proton hopping. 5,6,11,29 Exploring the mobility distribution across ionomer films can thus help us understand the observed distribution in the proton conduction (Figure 4) within the films.

We, therefore, incorporated rotor probe CCVJ within ionomer films to explore the mobility/stiffness distribution across ionomer films. To present the mobility/stiffness of a location within a film $(I_{z/d})$ relative to the substrate interface $(I_{z=0})$, we plotted $I_{z/d}/I_{z=0}$ as a function of z/d (Figure 5). $I_{z/d}/I_{z=0} > 1$ at any location (z/d) within a film thus indicated that that location (z/d) was stiffer relative to substrate interface (z=0).

At 25% RH, all films stiffened gradually and to almost a similar extent $(I_{z/d}/I_{z=0} \sim 1.3)$ up to about half-depth of the films (Figure 5a). As we moved beyond that point (i.e., z/d >0.5) and approached the air interface, thicker films (600-850 nm thick) began plasticizing and water-ionomer inside the films started to become more mobile. But thinner films (65-300 nm) showed a tendency to retain the low mobility/high stiffness until the air interface. The shear force acting during spin-coating of ionomer films^{2,49,13} and self-assembled features (e.g., ionomer micelle bundle) longer than film thickness 14,15 can preferentially align the ionomer backbones parallel to substrate and side chains (with -SO₃H groups) perpendicular to substrate as film thickness approaches ~50 nm.^{2,14} Such chain orientation may favor interfacial interactions among -SO₃H (Nafion), -SiOH (substrate), and water, and pin the ionomer chains and water molecules to the substrate. 3,6,50 If the major volume fraction of the film comprises such geometrically and interfacially constrained ionomer chains (e.g., 65 nm thick film), low segmental mobility of ionomers can propagate up to the air interface (Figure 5a). Conversely, polymer chains in relatively thicker films (>50 nm) prefer to adopt more isotropic conformation.^{2,14} Thus, the constraints imposed by substrate interface can impact a relatively smaller fraction of the film next to the substrate, while the air interface, being a substrate-free interface and away from the substrate, can impart more mobility to polymer chain segments and

water molecules in the region next to it.³⁷ This likely explains the onset of plasticization in thicker films above a certain value of z/d (Figure 4a). The fact that thinner films are stiffer at the air interface at low humidity is in agreement with the elastic modulus reported by others where 55–950 nm thick films were indented from 5 to 50% of their thickness from the top.⁵¹

Now, if the substrate interface alone was controlling the mobility, we should see the lowest mobility (highest $I_{z/d}/I_{z=0}$) next to the substrate interface or at least a flat mobility profile extending from substrate interface onward. 52 But we consistently saw hump-like mobility distribution curves indicating the lowest mobility in the middle of the films. We saw this hump-shaped curve even at the dry state (Figure S7), suggesting the lowest midzone mobility as a humidityindependent behavior. We attributed this to polymer chain density and entanglement. 39,53,54 As per neutron reflectometry, the midregion of Nafion films are more polymer-rich (layer density $\sim 1.59 - 1.83$ g/cm³ at 30% RH) than the region next to the substrate interface (~1.24 g/cm³).³⁴ Also, the spatially resolved entanglement density was found maximum in the middle of the polymer films.⁵⁴ Dense packing of entangled polymer chains can lower the chain mobility and stiffen the films. Additionally, some Nafion chains (isotropically oriented), bound to the substrate, can extend and reach to the middle of the film where their segmental mobility can be controlled by substrate remotely.55

Hydration stiffened the films further. For any film, $I_{z/d}/I_{z=0}$ at 88% RH became higher than that at 25% RH (Figure 5b), demonstrating the participation of water molecules in the stiffening processes. But the highest midzone stiffening/lowest midzone mobility ($I_{z/d}/I_{z=0}$ as high as 2, Figure 5b) could still be a combined effect of water—ionomer interaction, polymer chain density, and chain entanglement density. Importantly, the width of the antiplasticized region (Figure 5b) matched with that of the low $I_{\rm d}/I_{\rm p}$ region (Figure 4c) of a specific film. This clearly showed that water—polymer mobility has an important role in modulating proton conductivity.

However, the water—ionomer mobility may not solely determine the proton conduction behavior of these films.

For example, the mobility at air (z/d = 1) and substrate (z/d = 1)0) interfaces were not much different in ~600 nm thick film even at 88% RH (Figure 5b), but I_d/I_p was. Ionic conductivity is controlled by both mobility and concentration of charge carriers. Air interface, being more ionomer rich than substrate interface, 34,35 can have a higher concentration of charge carrier (-SO₃H) groups. We also estimated the availability of surface charge carrier groups in thick vs. thin films using surface elemental mapping (Figure 6). The sulfur-to-fluorine (S/F) ratio indicated that the surface of 850 nm thick Nafion film (S/ F = 0.09, Figure 6a,b,e) was more hydrophilic than the 250 nm thick one (S/F = 0.02, Figure 6c-e). Additionally, I_d/I_p is correlated to ionic domain size. 12 Together these facts made it evident that the hydrophilic charge carrier groups in close proximity, when formed larger ionic domains, higher I_d/I_p was favored, as seen in thicker films at the air interface.

In conclusion, our CLSM-based strategy can unravel the distribution of ion conduction, water-ionomer mobility/ stiffness across ionomer thin films and bulk membranes. CLSM-imaging of Nafion samples containing HPTS revealed a uniform proton conduction behavior across the bulk membrane, while both thickness- and interface-dependent proton conduction was observed across submicron thick films at controlled humidity. In submicron thick films, proton conduction (I_d/I_p) was always weak near substrate interface, then gradually increased until the air interface. The mobility/ stiffness distribution was also elucidated using the same strategy but using CCVJ. The width of the antiplasticized region near the substrate interface matched with that of the low I_d/I_p region of a film and demonstrated the critical role played by water-ionomer mobility on thin-film ionic conductivity. Earlier, we had to rely on an average value of proton conductivity for an entire ionomer sample. The CLSMbased strategy now allows us to reveal how the ionic conductivity is at different depths and how far the interfacial effects propagate inside very thin films. Such information will guide us to design catalyst layers for electrochemical devices.

ASSOCIATED CONTENT

Supporting Information

The Supporting Information is available free of charge at https://pubs.acs.org/doi/10.1021/acsmacrolett.1c00110.

Experimental details; Figures S1-S7 (PDF)

AUTHOR INFORMATION

Corresponding Author

Shudipto K. Dishari — Department of Chemical and Biomolecular Engineering, University of Nebraska—Lincoln, Lincoln, Nebraska 68588, United States; orcid.org/0000-0003-1679-2332; Phone: 402-472-7537; Email: sdishari2@unl.edu

Authors

Seefat Farzin — Department of Chemical and Biomolecular Engineering, University of Nebraska—Lincoln, Lincoln, Nebraska 68588, United States

Ehsan Zamani — Department of Chemical and Biomolecular Engineering, University of Nebraska—Lincoln, Lincoln, Nebraska 68588, United States

Complete contact information is available at: https://pubs.acs.org/10.1021/acsmacrolett.1c00110

Notes

The authors declare no competing financial interest.

ACKNOWLEDGMENTS

S.K.D. acknowledges the supports from the NSF CAREER Award (NSF-DMR #1750040), Nebraska EPSCoR First Award, and UNL start-up funding. The CLSM images were taken at the Microscopy Core Facility of the Nebraska Center for Biotechnology. Part of the research (surface elemental mapping) was performed in the Nebraska Nanoscale Facility: National Nanotechnology Coordinated Infrastructure and the Nebraska Center for Materials and Nanoscience, which are supported by the National Science Foundation under Award NNCI-1542182, and the Nebraska Research Initiative. S.K.D. thanks Dr. Anandakumar Sarella for helping us with the surface chemical mapping in SEM.

REFERENCES

- (1) Holdcroft, S. Fuel Cell Catalyst Layers: A Polymer Science Perspective. *Chem. Mater.* **2014**, *26*, 381–393.
- (2) Kusoglu, A.; Weber, A. Z. New Insights into Perfluorinated Sulfonic Acid Ionomers. *Chem. Rev.* **2017**, *117*, 987–1104.
- (3) Paul, D. K.; McCreery, R.; Karan, K. Proton Transport Property in Supported Nafion Nanothin Films by Electrochemical Impedance Spectroscopy. *J. Electrochem. Soc.* **2014**, *161*, F1395–F1402.
- (4) Karan, K. Interesting Facets of Surface, Interfacial, and Bulk Characteristics of Perfluorinated Ionomer Films. *Langmuir* **2019**, *35*, 13489–13520.
- (5) Dishari, S. K.; Hickner, M. A. Antiplasticization and Water Uptake of Nafion® Thin Films. ACS Macro Lett. 2012, 1, 291–295.
- (6) Dishari, S. K.; Hickner, M. A. Confinement and Proton Transfer in Nafion Thin Films. *Macromolecules* **2013**, *46*, 413–421.
- (7) Arges, C. G.; Kambe, Y.; Dolejsi, M.; Wu, G. P.; Segal-Pertz, T.; Ren, J.; Cao, C.; Craig, G. S. W.; Nealey, P. F. Interconnected Ionic Domains Enhance Conductivity in Microphase Separated Block Copolymer Electrolytes. *J. Mater. Chem. A* **2017**, *5*, 5619–5629.
- (8) Dishari, S. K. Current Understanding of Proton Conduction in Confined Ionomeric Systems. *J. Postdoc. Res.* **2014**, *2*, 30–39.
- (9) Modestino, M. A.; Paul, D. K.; Dishari, S.; Petrina, S. A.; Allen, F. I.; Hickner, M. A.; Karan, K.; Segalman, R. A.; Weber, A. Z. Self-Assembly and Transport Limitations in Confined Nafion Films. *Macromolecules* **2013**, *46*, 867–873.
- (10) Allen, F. I.; Comolli, L. R.; Kusoglu, A.; Modestino, M. A.; Minor, A. M.; Weber, A. Z. Morphology of Hydrated As-Cast Nafion Revealed through Cryo Electron Tomography. *ACS Macro Lett.* **2015**, 4, 1–5.
- (11) Farzin, S.; Johnson, T. J.; Chatterjee, S.; Zamani, E.; Dishari, S. K. Ionomers From Kraft Lignin for Renewable Energy Applications. *Front. Chem.* **2020**, *8*, 690.
- (12) Farzin, S.; Sarella, A.; Yandrasits, M. A.; Dishari, S. K. Fluorocarbon-Based Ionomers with Single Acid and Multiacid Side Chains at Nanothin Interfaces. *J. Phys. Chem. C* **2019**, *123*, 30871–30884
- (13) Dishari, S. K.; Rumble, C. A.; Maroncelli, M.; Dura, J. A.; Hickner, M. A. Unraveling the Complex Hydration Behavior of Ionomers under Thin Film Confinement. *J. Phys. Chem. C* **2018**, *122*, 3471–3481.
- (14) Kushner, D. I.; Kusoglu, A.; Podraza, N. J.; Hickner, M. A. Substrate-Dependent Molecular and Nanostructural Orientation of Nafion Thin Films. *Adv. Funct. Mater.* **2019**, *29*, 1902699.
- (15) Zimudzi, T. J.; Hickner, M. A. Signal Enhanced FTIR Analysis of Alignment in NAFION Thin Films at SiO2 and Au Interfaces. *ACS Macro Lett.* **2016**, *5*, 83–87.
- (16) Kusoglu, A.; Kushner, D.; Paul, D. K.; Karan, K.; Hickner, M. A.; Weber, A. Z. Impact of Substrate and Processing on Confinement of Nafion Thin Films. *Adv. Funct. Mater.* **2014**, 24, 4763–4774.

- (17) Page, K. A.; Shin, J. W.; Eastman, S. A.; Rowe, B. W.; Kim, S.; Kusoglu, A.; Yager, K. G.; Stafford, G. R. In Situ Method for Measuring the Mechanical Properties of Nafion Thin Films during Hydration Cycles. ACS Appl. Mater. Interfaces 2015, 7, 17874–17883.
- (18) Frieberg, B. R.; Page, K. A.; Graybill, J. R.; Walker, M. L.; Stafford, C. M.; Stafford, G. R.; Soles, C. L. Mechanical Response of Thermally Annealed Nafion Thin Films. *ACS Appl. Mater. Interfaces* **2016**, *8*, 33240–33249.
- (19) Ellison, C. J.; Torkelson, J. M. The Distribution of Glass-Transition Temperatures in Nanoscopically Confined Glass Formers. *Nat. Mater.* **2003**, *2*, 695–700.
- (20) Roth, C. B.; Mcnerny, K. L.; Jager, W. F.; Torkelson, J. M. Eliminating the Enhanced Mobility at the Free Surface of Polystyrene: Fluorescence Studies of the Glass Transition Temperature in Thin Bilayer Films of Immiscible Polymers. *Macromolecules* **2007**, *40*, 2568–2574.
- (21) Baglay, R. R.; Roth, C. B. Experimentally Determined Profile of Local Glass Transition Temperature across a Glassy-Rubbery Polymer Interface with a Tg Difference of 80 K. J. Chem. Phys. 2015, 143, 111101.
- (22) Miller, K. E.; Krueger, R. H.; Torkelson, J. M. Mobility-Sensitive Fluorescence Probes for Quantitative Monitoring of Water Sorption and Diffusion in Polymer Coatings. *J. Polym. Sci., Part B: Polym. Phys.* **1995**, *33*, 2343–2349.
- (23) Haidekker, M. A.; Brady, T. P.; Lichlyter, D.; Theodorakis, E. A. A Ratiometric Fluorescent Viscosity Sensor. *J. Am. Chem. Soc.* **2006**, *128*, 398–399.
- (24) Haidekker, M. A.; Nipper, M.; Mustafic, A.; Lichlyter, D.; Dakanali, M.; Theodorakis, E. A. Dyes with Segmental Mobility: Molecular Rotors. *Advanced Fluorescence Reporters in Chemistry and Biology*; Springer, 2010; pp 267–308.
- (25) Tanaka, K.; Chujo, Y. Advanced Functional Materials Based on Polyhedral Oligomeric Silsesquioxane (POSS). *J. Mater. Chem.* **2012**, 22, 1733–1746.
- (26) Haidekker, M. A.; Lichlyter, D.; Johny, M. B.; Grimes, C. A. Probing Polymerization Dynamics with Fluorescent Molecular Rotors and Magnetoelastic Sensors. *Sens. Lett.* **2006**, *4*, 257–261.
- (27) Hawe, A.; Filipe, V.; Jiskoot, W. Fluorescent Molecular Rotors as Dyes to Characterize Polysorbate-Containing IgG Formulations. *Pharm. Res.* **2010**, 27, 314–326.
- (28) Moilanen, D. E.; Levinger, N. E.; Spry, D. B.; Fayer, M. D. Confinement or the Nature of the Interface? Dynamics of Nanoscopic Water. *J. Am. Chem. Soc.* **2007**, *129*, 14311–14318.
- (29) Spry, D. B.; Goun, A.; Glusac, K.; Moilanen, D. E.; Fayer, M. D. Proton Transport and the Water Environment in Nafion Fuel Cell Membranes and AOT Reverse Micelles. *J. Am. Chem. Soc.* **2007**, *129*, 8122–8130.
- (30) Moilanen, D. E.; Spry, D. B.; Fayer, M. D. Water Dynamics and Proton Transfer in Nafion Fuel Cell Membranes. *Langmuir* **2008**, *24*, 3690–3698.
- (31) Fayer, M. D. Dynamics of Water Interacting with Interfaces, Molecules, and Ions. Acc. Chem. Res. 2012, 45, 3-14.
- (32) Fayer, M. D.; Levinger, N. E. Analysis of Water in Confined Geometries and at Interfaces. *Annu. Rev. Anal. Chem.* **2010**, *3*, 89–107
- (33) Spry, D. B.; Fayer, M. D. Proton Transfer and Proton Concentrations in Protonated Nafion Fuel Cell Membranes. *J. Phys. Chem. B* **2009**, *113*, 10210–10221.
- (34) Kawamoto, T.; Aoki, M.; Kimura, T.; Mizusawa, T.; Yamada, N. L.; Miyake, J.; Miyatake, K.; Inukai, J. In-Plane Distribution of Water inside Nafion Thin Film Analyzed by Neutron Reflectivity at Temperature of 80 °C and Relative Humidity of 30–80% Based on 4-Layered Structural Model. *Jpn. J. Appl. Phys.* **2019**, *58*, SIID01–5.
- (35) Kawamoto, T.; Aoki, M.; Kimura, T.; Chinapang, P.; Mizusawa, T.; Yamada, N. L.; Nemoto, F.; Watanabe, T.; Tanida, H.; Matsumoto, M.; Imai, H.; Miyake, J.; Miyatake, K.; Inukai, J. Sublayered Structures of Hydrated Nafion® Thin Film Formed by Casting on Pt Substrate Analyzed by X-Ray Absorption Spectroscopy under Ambient Conditions and Neutron Reflectometry at Temper-

- ature of 80 °C and Realtive Humidity of 30-80%. *Electrochemistry* **2019**, 87, 270-275.
- (36) Baglay, R. R.; Roth, C. B. Local Glass Transition Temperature Tg (z) of Polystyrene next to Different Polymers: Hard vs. Soft Confinement. *J. Chem. Phys.* **2017**, *146*, 203307.
- (37) Glor, E. C.; Angrand, G. V.; Fakhraai, Z. Exploring the Broadening and the Existence of Two Glass Transitions Due to Competing Interfacial Effects in Thin, Supported Polymer Films. *J. Chem. Phys.* **2017**, *146*, 203330.
- (38) Dura, J. A.; Murthi, V. S.; Hartman, M.; Satija, S. K.; Majkrzak, C. F. Multilamellar Interface Structures in Nafion. *Macromolecules* **2009**, 42, 4769–4774.
- (39) Decaluwe, S. C.; Baker, A. M.; Bhargava, P.; Fischer, J. E.; Dura, J. A. Structure-Property Relationships at Nafion Thin-Film Interfaces: Thickness Effects on Hydration and Anisotropic Ion Transport. *Nano Energy* **2018**, *46*, 91–100.
- (40) Hwang, G. S.; Parkinson, D. Y.; Kusoglu, A.; MacDowell, A. A.; Weber, A. Z. Understanding Water Uptake and Transport in Nafion Using X-Ray Microtomography. *ACS Macro Lett.* **2013**, *2*, 288–291.
- (41) Komini Babu, S.; Chung, H. T.; Zelenay, P.; Litster, S. Resolving Electrode Morphology's Impact on Platinum Group Metal-Free Cathode Performance Using Nano-CT of 3D Hierarchical Pore and Ionomer Distribution. ACS Appl. Mater. Interfaces 2016, 8, 32764–32777.
- (42) Wang, C.; Lee, D. H.; Hexemer, A.; Kim, M. I.; Zhao, W.; Hasegawa, H.; Ade, H.; Russell, T. P. Defining the Nanostructured Morphology of Triblock Copolymers Using Resonant Soft X-Ray Scattering. *Nano Lett.* **2011**, *11*, 3906–3911.
- (43) Culp, T. E.; Ye, D.; Paul, M.; Roy, A.; Behr, M. J.; Jons, S.; Rosenberg, S.; Wang, C.; Gomez, E. W.; Kumar, M.; Gomez, E. D. Probing the Internal Microstructure of Polyamide Thin-Film Composite Membranes Using Resonant Soft X-Ray Scattering. *ACS Macro Lett.* **2018**, *7*, 927–932.
- (44) Liu, F.; Brady, M. A.; Wang, C. Resonant Soft X-Ray Scattering for Polymer Materials. *Eur. Polym. J.* **2016**, *81*, 555–568.
- (45) Hwang, M.; Nixon, K.; Sun, R.; Willis, C.; Elabd, Y. A. Sulfonated Pentablock Terpolymers as Membranes and Ionomers in Hydrogen Fuel Cells. *J. Membr. Sci.* **2021**, *633*, 119330.
- (46) Bass, M.; Freger, V. Hydration of Nafion and Dowex in Liquid and Vapor Environment: Schroeder's Paradox and Microstructure. *Polymer* **2008**, *49*, 497–506.
- (47) Bass, M.; Berman, A.; Singh, A.; Konovalov, O.; Freger, V. Surface Structure of Nafion in Vapor and Liquid. *J. Phys. Chem. B* **2010**, *114*, 3784–3790.
- (48) Bass, M.; Berman, A.; Singh, A.; Konovalov, O.; Freger, V. Surface-Induced Micelle Orientation in Nafion Films. *Macromolecules* **2011**, *44*, 2893–2899.
- (49) Hill, T. A.; Carroll, D. L.; Czerw, R.; Martin, C. W.; Perahia, D. Atomic Force Microscopy Studies on the Dewetting of Perfluorinated Ionomer Thin Films. *J. Polym. Sci., Part B: Polym. Phys.* **2003**, *41*, 149–158.
- (50) Mckechnie, D.; Cree, J.; Wadkin-snaith, D.; Johnston, K. Glass Transition Temperature of a Polymer Thin Film: Statistical and Fitting Uncertainties. *Polymer* **2020**, *195*, 122433.
- (51) Nadermann, N. K.; Davis, E. M.; Page, K. A.; Stafford, C. M.; Chan, E. P. Using Indentation to Quantify Transport Properties of Nanophase-Segregated Polymer Thin Films. *Adv. Mater.* **2015**, *27*, 4924–4930.
- (52) Zhang, W.; Douglas, J. F.; Starr, F. W. Why We Need to Look beyond the Glass Transition Temperature to Characterize the Dynamics of Thin Supported Polymer Films. *Proc. Natl. Acad. Sci. U. S. A.* **2018**, *115*, 5641–5646.
- (53) Nie, Y.; Zhou, Z.; Hao, T.; Ye, X.; Yang, W. The Distribution of Glass Transition Temperatures in Ultrathin Polymer Films Controlled by Segment Density or Interfacial Interaction. *Macromol. Theory Simul.* **2016**, 25, 187–195.
- (54) García, N. A.; Barrat, J. L. Entanglement Reduction Induced by Geometrical Confinement in Polymer Thin Films. *Macromolecules* **2018**, *51*, 9850–9860.

(55) Siretanu, I.; Chapel, J. P.; Drummond, C. Substrate Remote Control of Polymer Film Surface Mobility. *Macromolecules* **2012**, *45*, 1001–1005.